Journal of Computational Applied Mechanics 2026, 57(4): 752-773
DOI: 10.22059/jcamech.2026.424028.1977

RESEARCH PAPER

Magnetically tuned vortex dynamics and thermal transport in a hybrid nanofluid-filled lid-driven cavity

Shabbir Ahmad [a], Kashif Ali [b], Farhan Lafta Rashid [c], Sherain Mohamed [d,*] Mahmoud M Selim [d], Blgys A. Muflh [d]

[a] *Graduate Program of Ocean Engineering, School of Engineering, Universidade Federal do Rio Grande - FURG, Rio Grande, 96201-900, Brasil*
[n] *Center for Computational Sciences - C3, Universidade Federal do Rio Grande - FURG, Rio Grande, 96201-900, Brasil*
[c] *Petroleum Engineering Department, College of Engineering, University of Kerbala, Karbala 56001, Iraq*
[d] *Department of Mathematics, College of Science and Humanities, Prince Sattam bin Abdulaziz University, P.O. Box 710, Al-Kharj 11942, Saudi Arabia*

Abstract

Efficient control of fluid mixing and heat transport is a major challenge in modern thermal engineering systems, including electronic cooling devices, heat exchangers, thermal energy storage units, and industrial processing equipment. In lid-driven cavities, vortex formation plays a fundamental role in improving convective heat transfer by enhancing fluid circulation and promoting thermal mixing between hot and cold regions. The introduction of localized magnetic fields provides an additional mechanism for controlling these vortical structures through Lorentz-force-driven flow modification. In electrically conducting hybrid nanofluids, the interaction between the magnetic field and fluid motion can significantly alter vortex dynamics, leading to enhanced thermal transport and improved heat transfer performance. Motivated by these practical and scientific considerations, the present study numerically investigates the influence of localized magnetic fields on vortex formation and heat transfer enhancement inside a two-dimensional lid-driven cavity filled with Ag–Fe_3O_4/water hybrid nanofluid. The governing equations are transformed into dimensionless form using the stream–vorticity formulation and solved through the Alternating Direction Implicit (ADI) scheme. The effects of the magnetic interaction parameter (Mn), Reynolds number (Re), magnetic strip width (L), and nanoparticle volume fractions on streamline structures, isotherms, skin friction coefficient, and Nusselt number are examined. The results reveal that localized magnetic fields significantly modify vortex dynamics and thermal transport within the cavity. Increasing the magnetic interaction parameter strengthens Lorentz-force-induced recirculation zones and improves thermal mixing near the magnetic strips. The Reynolds number considerably enhances convective heat transfer, while the magnetic strip width strongly influences vortex interaction and heat transfer enhancement. The average Nusselt number efficiency increases by approximately 354% with increasing Reynolds number and by about 30% for optimized magnetic strip width. Furthermore, increasing nanoparticle concentration substantially improves the thermal performance of the hybrid nanofluid. The findings demonstrate that localized magnetic fields provide an effective mechanism for controlling vortex structures and enhancing heat transfer in hybrid nanofluid-filled enclosures.

Keywords: Hybrid nanofluids; Vortex Formation; Nanofluidic; Efficiency; Single-phase model; Localized magnetic field.

[*] Corresponding Author: sm.mohamd@psau.edu.as

1. Introduction

Traditional working fluids have been slowly replaced by advanced fluids having better heat transfer properties in recent years in thermal systems. The advent of nanotechnology has ushered in the new nanofluids as an effective method to improve the thermal performance in different engineering fields. The conjugate free convection of nanofluids with sinusoidal temperature conditions has been explored by the researchers of Alsabery et al. [1]. They pointed out that the variation in thermal boundaries affects the heat transfer properties. Selimefendigil and Öztop [2] studied conjugate convection of nanofluids in an enclosure and found that the temperature difference rises as the Grashof number rises. Garoosi et al. [3] analyzed free convection of a nanofluid in a heat exchanger configuration using the Buongiorno model. Sheikholeslami and his colleagues [4] added magnetic and radiation source terms to their analysis and showed that the magnetic field reduces the temperature gradient. In general, many recent investigations have been directed towards the study of nanofluid heat transfer under the action of a magnetic field [5-7]. The studies confirmed that the magnetic forces, the property of nanoparticles, and the flow condition have a significant impact on the motion of fluids, heat transfer enhancement, and thermal transport in various engineering systems. Ayub et al. [8] studied electromagnetohydrodynamic boundary layer flow and solved the problem numerically using the shooting method. In the study conducted by Shehzad et al. [9], a wavy duct was used to examine the flow of a nanofluid under the effects of Brownian motion by applying the Nelder–Mead optimization technique. Bhatti et al. [10] investigated the entropy generation of the nanofluid flow in a porous plate and found that entropy production increases with the increase in the intensity of the thermophoresis and thermal radiation effects. Sheikholeslami et al. [11] examined the flow of nanofluid together with an induced magnetic field using the Buongiorno model. Another study by Sheikholeslami and Ganji [12] used a semi-analytical method to examine the heat transfer of a nanofluid under induced magnetic fields, considering the Joule heating effects in the energy equation. The effects of the Hartmann number and nanoparticle concentration on heat transport and entropy generation in a Darcy–Forchheimer porous cavity filled with a copper–water nanofluid were investigated by Marzougui et al. [13]. They focused their research on the mixed-convection and irreversible behavior of the magnetic field. The numerical analysis was conducted by finite elements and the Darcy–Brinkman–Forchheimer model. The investigation disclosed that the flow over a horizontal wall significantly affects entropy generation and that thermal entropy generation is nearly linearly proportional to the nanoparticle volume fraction. Korei et al. [14] numerically performed the magneto-convection phenomena of Al2O3-Cu/water hybrid nanofluid in an enclosure with rounded corners. The cavity was partially heated from the bottom wall, and the analysis was performed by means of computational fluid dynamics techniques. The results showed that the direction of the magnetic field was a significant parameter in the temperature and fluid flow. The magnetic field was more effective when applied perpendicular to gravity to achieve better heat transport performance. Also, the heat transfer was reduced, and the irreversibility within the enclosure was minimized by decreasing the corner radius.

The study of heat transfer and fluid flow in lid-driven cavities has attracted considerable attention because of its wide range of engineering and industrial applications. There are also several studies specifically studying heat transfer mechanisms in lid-driven enclosures. Prasad & Koseff [15] examined mixed convection heat transfer within an insulated rectangular cavity driven by a moving lid. The lid was moving to create forced convection, and the upper wall was cooled, whereas the lower wall was heated to create natural convection. This detailed insight into the thermal behavior under various operating conditions was gained by flow visualization and heat flux measurement. Correlations for the Nusselt and Stanton numbers were also developed for engineering design applications. Luo & Yang [16] studied a continuation method to investigate the flow bifurcation and thermal transport in a lid-driven cavity. The lower and upper lids were in opposite movement and were at different temperatures. A detailed bifurcation diagram was created by the authors, and linear stability analysis was performed to find the various flow regimes and thermal transport characteristics. The heat transfer and nonequilibrium gaseous flow within a cavity driven by a lid were studied by John et al. [17] with the direct simulation Monte Carlo method. They worked in the slip regime to the free molecular regime. The study identified complex thermal transport phenomena that are not well represented by the classical Navier–Stokes equations, such as counter-gradient heat transfer and viscous dissipation effects. The flow in a square cavity produced by the movement of the buoyancy effect, and the upper lid caused by the heating of the bottom surface, was investigated by Moallemi & Jang [18]. The motivation for the work was applications in the glass manufacturing processes. Numerical simulations were carried out for laminar flow with respect to Reynolds and Prandtl numbers. The outcomes revealed that there was a significant interaction between natural and forced convection mechanisms.

Khanafer [19] performed an analytical study of heat transfer in an enclosure with flexible and wavy heated bottom walls using a numerical approach. The Galerkin FEM formulation was used to solve the governing equations. The research found that the wavy wall configuration can enhance heat transfer performance more than the flat wall cases. This forced and natural convection interaction was also a significant influence on the deformation of the walls and the transport of thermal energy within the cavity. Chatterjee et al. [20] examined the mixed convection transport in an enclosure with a thermally insulated rotating circular cylinder at the center. The nanofluid Cu–water was filled in the enclosure. They concluded that heat transfer and the flow are under natural convection at high Richardson numbers, and forced convection at low Richardson numbers. Besides, the drag coefficient and Nusselt number are found to be increasing with the cylinder rotation speed and Richardson number. Roslan et al. [21] investigated the heat transfer and flow of mixed convection in an obstructed cavity with a rotating cylinder and filled with nanofluid. The investigation showed that the higher the concentration of the nanoparticles, the better the heat transport performance. Also, the cylinder rotation speed boosted the level of thermal distribution inside the cavity, and the cylinder size had a significant impact on the flow structure and the fluid behavior. Coste and Raimundo [22] studied numerically combined convection heat transfer in a differentially heated square cavity filled with a centrally spinning cylinder. They studied the effect of cylinder size and rotational speed. The results indicated that these parameters play vital roles in the flow and thermal characteristics within the enclosure. In conclusion, the literature review reveals that only a few studies have focused on the heat convection in the cavity filled with nanofluids with the presence of internal rotating cylinders [23-25]. The majority of these studies concentrated on the effects of the type and concentration of the nanoparticles, the particle size, and the geometric and rotational effects of the internal cylinders on heat transfer enhancement and flow behavior.

The study of magnetohydrodynamic free convection has been a subject of much attention due to its many engineering applications, such as electronic cooling, combustion processes, fire safety engineering, and thermal management technologies. Verma & Das [26] considered the ferrofluid flow in an external magnetic field within an enclosure. They studied the influence of aspect ratio, Reynolds number, and intensity of a magnetic field on the generation of vortices and flow behavior. It was revealed that a magnetic field has a significant impact on vortex structure, stability, and distribution of vorticity inside the cavity. The flow pattern gradually morphed from a simple recirculation cell to more complex vortex types. The results could have implications for microfluidics, drug delivery systems, and flow control devices. Mahmuda Maya et al. [27] studied the magnetohydrodynamic hybrid convection with a rectangular heat source in an enclosure. The effect of the size of the heat source, heat absorption or generation, and the strength of a magnetic field was studied. The results revealed that the higher the size of the heat source and magnetic field intensity, the lower the average Nusselt number, and the higher the heat absorption, the better the thermal performance. Maneengam et al. [28] considered the role of the entropy generation and mixed convection of Fe3O4-MWCNT/water nanofluid in a permeable cubic enclosure. The cavity had wavy side walls and a moving top lid under the magnetic field effect. Their results indicated that magnetic forces have a significant effect on thermal and flow properties. Thermal distribution was increased with the application of a magnetic field when it was applied at a right angle to the flow direction at higher Reynolds numbers. Furthermore, a reduction in the Reynolds number and a rise in the Hartmann number resulted in decreasing the rate of heat transfer as well as irreversibility. Hasan et al. [29] studied the time-dependent mixed convection flow in a two-dimensional enclosure with CNT–kerosene nanofluid. The study included the effects of magnetohydrodynamics and thermal radiation. The nonlinear dimensionless equations were solved using Galerkin FDM (finite element method). It was found that the drag force and pressure gradient increases in the natural convection condition, while the Nusselt number surges with the increase of the dimensionless time and Richardson number. Hussain et al. [30] analyzed the magneto-bioconvection flow of hybrid nanofluid inside a porous cavity filled with gyrotactic microorganisms and a streamlined obstacle. Numerical outcomes showed that the heat transfer rate is almost constant with the increase of the Peclet number, and the Sherwood number decreases with increasing the Peclet number. The dimensions of the obstacles are effective as a control parameter and have opposite effects on heat transfer properties. Herouz et al. [31] numerically investigated the mixed convection flow of nano-encapsulated phase change material (NEPCM) in a porous hexagonal cavity with double lid-driven walls. The top and bottom walls were moving at the same speed, and there was a heated square obstacle inside the enclosure. Numerical solution was obtained using Galerkin finite element method. The results indicated that the fluid flow and the thermal transport are reduced when the cavity permeability is decreased. Furthermore, high magnetic fields have a negative influence on heat transfer and the circulation of fluids.

Novelty: The novelty of the present work lies in the investigation of localized magnetic-field-induced vortex formation and its influence on heat transfer enhancement inside a lid-driven cavity filled with hybrid nanofluids. Unlike conventional magnetohydrodynamic studies that mainly consider uniformly distributed magnetic fields, the current study introduces strategically positioned localized magnetic strips to actively manipulate vortex dynamics and thermal transport behavior. The combined effects of magnetic interaction strength, strip width, Reynolds number, and hybrid nanoparticle concentration on flow circulation and heat transfer are comprehensively analyzed using the Alternating Direction Implicit (ADI) numerical scheme, and the stream–vorticity formulation. Furthermore, the study provides a detailed characterization of Lorentz-force-driven recirculation zones and demonstrates how localized magnetic fields can be utilized to optimize convective heat transfer performance. The incorporation of hybrid nanoparticles together with localized magnetic control offers a new framework for enhancing thermo-hydrodynamic performance in advanced cooling and thermal management applications.

2. Problem Description

Fig. 1 illustrates the physical configuration of a two-dimensional cavity, where a localized magnetic field is strategically applied through separate vertical strips. The arrows show how the magnetic field is applied in the domain of the cavity. The interaction between the swirling nanofluid and the magnetic field generates Lorentz forces, which significantly influence vortex formation, fluid mixing, and heat transfer characteristics. This configuration plays a crucial role in governing flow dynamics, as well as enhancing oxygen distribution and microorganism transport within the enclosure.

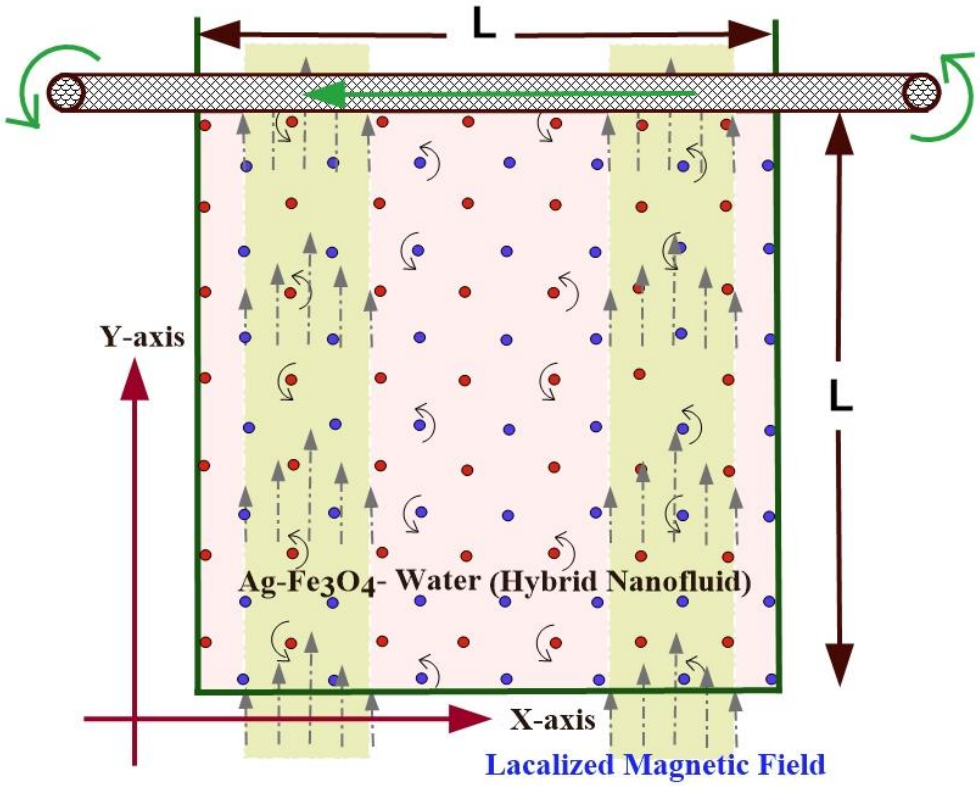

Fig. 1. Schematic Model

The current study is under the following assumptions:

- Incompressible and laminar flow is considered.
- The nanofluid-based micropolar fluid saturated with Ag and SWCNT nanoparticles is considered, and the effect of microrotation is included.
- A spatially varying magnetic field is taken to be uniform in the magnetized strip regions.
- No-slip boundary conditions are applied to all the enclosure walls.

- The horizontal top and bottom lids are in opposite directions.

The magnetic field (H), produced by horizontal and vertical strips, is given below:

$$\tilde{H}_1(x,y) = H_0\left\{\tanh A_1'\left(x-x_1\right) - \tanh A_2'\left(x-x_2\right)\right\},$$
$$\tilde{H}_2(x,y) = H_0\left\{\tanh A_1'\left(x-x_3\right) - \tanh A_2'\left(x-x_4\right)\right\}, \quad (1)$$

and

$$H = \tilde{H}_1(x,y) + \tilde{H}_2(x,y)$$

The magnetic field is restricted inside a strip, which is defined by $x_1 \le x \le x_2,\ x_3 \le x \le x_4;\ 0 \le y \le L$ correspondingly.

3. Mathematical Formulation

In dimensional terms, the equations are expressed as follows. [32]:

$$\frac{\partial \tilde{U}}{\partial x} + \frac{\partial \tilde{V}}{\partial y} = 0, \quad (2)$$

$$\frac{\partial \tilde{U}}{\partial t'} + \left(\tilde{V}\frac{\partial \tilde{U}}{\partial y} + \tilde{U}\frac{\partial \tilde{U}}{\partial x}\right) = -\frac{1}{\hat{\rho}_{hnf}}\frac{\partial P}{\partial x} + \left(\hat{\upsilon}_{hnf} + \frac{\kappa}{\rho}\right)\left(\frac{\partial^2 \tilde{U}}{\partial y^2} + \frac{\partial^2 \tilde{U}}{\partial x^2}\right) + \frac{\bar{\mu}_o \tilde{M}}{\hat{\rho}_{hnf}}\frac{\partial \tilde{H}}{\partial x}, \quad (3)$$

$$\frac{\partial \tilde{V}}{\partial t'} + \left(\tilde{U}\frac{\partial \tilde{V}}{\partial x} + \tilde{V}\frac{\partial \tilde{V}}{\partial y}\right) = -\frac{1}{\hat{\rho}_{hnf}}\frac{\partial P}{\partial y} + \left(\hat{\upsilon}_{hnf} + \frac{\kappa}{\rho}\right)\left(\frac{\partial^2 \tilde{V}}{\partial x^2} + \frac{\partial^2 \tilde{V}}{\partial y^2}\right) + \frac{\bar{\mu}_o \tilde{M}}{\hat{\rho}_{hnf}}\frac{\partial \tilde{H}}{\partial y}, \quad (4)$$

$$\frac{\partial T}{\partial t'} + \frac{\left(\hat{\rho}c_p\right)_{hnf}}{k_{hnf}}\left(\tilde{U}\frac{\partial T}{\partial x} + \tilde{V}\frac{\partial T}{\partial y}\right) + \left(\frac{\bar{\mu}_o}{k_{hnf}}\right)T\frac{\partial \tilde{M}}{\partial T}\left(\tilde{V}\frac{\partial \tilde{H}}{\partial y} + \tilde{U}\frac{\partial \tilde{H}}{\partial x}\right)$$
$$= \nabla^2 T + \left(\frac{\tilde{\mu}_{hnf}}{k_{hnf}}\right)\left\{2\left(\frac{\partial \tilde{U}}{\partial x}\right)^2 + \left(\frac{\partial \tilde{V}}{\partial x} + \frac{\partial \tilde{U}}{\partial y}\right)^2 + 2\left(\frac{\partial \tilde{V}}{\partial y}\right)^2\right\}. \quad (6)$$

By eliminating the pressure gradient term, the governing equations are reduced to the following simplified form:

$$\frac{\partial}{\partial t'}\left(\frac{\partial \tilde{U}}{\partial y} - \frac{\partial \tilde{V}}{\partial x}\right) + \hat{V}\frac{\partial}{\partial y}\left(\frac{\partial \tilde{U}}{\partial y} - \frac{\partial \tilde{V}}{\partial x}\right) + \tilde{U}\frac{\partial}{\partial x}\left(\frac{\partial \tilde{U}}{\partial y} - \frac{\partial \tilde{V}}{\partial x}\right)$$
$$= \hat{\upsilon}_{hnf}\left(\frac{\partial^2}{\partial x^2} + \frac{\partial^2}{\partial y^2}\right)\left(\frac{\partial \tilde{U}}{\partial y} - \frac{\partial \tilde{V}}{\partial x}\right) + \left(\frac{\partial\left(\frac{\bar{\mu}_0 \tilde{M}}{\hat{\rho}_{hnf}}\frac{\partial \tilde{H}}{\partial x}\right)}{\partial y} - \frac{\partial\left(\frac{\bar{\mu}_0 \tilde{M}}{\hat{\rho}_{hnf}}\frac{\partial \tilde{H}}{\partial y}\right)}{\partial x}\right). \quad (7)$$

6.1 Boundary Conditions

Right and left vertical walls (adiabatic):

$$\left.\begin{aligned} &\tilde{U}(0,y) = \tilde{U}(L,y) = 0,\ \left(\frac{\partial T}{\partial x}\right)_{x=0} = \left(\frac{\partial T}{\partial x}\right)_{x=L} = 0, \\ &\tilde{V}(0,y) = \tilde{V}(L,y) = 0;\ \ \hat{\varphi}(0,y) = \hat{\varphi}(L,y) = 0; \end{aligned}\right\} \quad 0 < y < L \quad (8a)$$

Lower Horizontal Wall:

$$\left.\begin{matrix}\tilde{U}(x,0)=0,\ T(x,0)=T_h,\\ \tilde{V}(x,0)=0;\ \tilde{\varphi}(x,0)=0\end{matrix}\right\} \quad 0<x<L. \tag{8b}$$

Upper Horizontal Wall:

$$\left.\begin{matrix}\tilde{U}(x,L)=-V_0,\quad T(x,L)=T_C,\\ \tilde{V}(x,L)=0;\ \ \tilde{\varphi}(x,L)=0\end{matrix}\right\} \quad 0<x<L \tag{8c}$$

The thermophysical characteristics of hybrid-based nanofluids, which are vital in the heat transfer process, are discussed. This investigation is focused on the density, specific heat, viscosity, and thermal conductivity of Cu-Fe_3O_4 nanoparticles, using correlations and data reported in the literature [33-37]. To carry out the analysis, the subsequent dimensionless variables are introduced:

$$\xi=\frac{x}{\tilde{L}},\ \eta=\frac{y}{\tilde{L}},\ u=\frac{\tilde{U}}{V_0},\ v=\frac{\tilde{V}}{V_0},\ \hat{\theta}=\frac{T-T_c}{\Delta T},\ H=\frac{\tilde{H}}{H_0},\ t=\frac{V_0}{\tilde{L}}t' \tag{9}$$

With the help of equations (5) and (6), the following relations can be obtained:

$$\frac{\partial J}{\partial t}+u\frac{\partial J}{\partial \xi}+v\frac{\partial J}{\partial \eta}=\left(\hat{\rho}_{hnf}\Big/\hat{\rho}_f\right)\left(\mu_f\Big/\mu_{hnf}\right)\frac{1}{\mathrm{Re}}\nabla^2 J+\frac{Mn}{\left(\hat{\rho}_{hnf}\Big/\hat{\rho}_f\right)}H\left(\frac{\partial H}{\partial \eta}.\frac{\partial \hat{\theta}}{\partial \xi}-\frac{\partial H}{\partial \xi}.\frac{\partial \hat{\theta}}{\partial \eta}\right), \tag{10}$$

$$\begin{aligned}\nabla^2\hat{\theta}=&\ \mathrm{Pr}*\left(\hat{\rho}_{hnf}\Big/\hat{\rho}_f\right)\left(\frac{\mu_f}{\mu_{hnf}}\right)*\left(\frac{(\hat{\rho}c_p)_{hnf}}{(\hat{\rho}c_p)_f}\right)\mathrm{Re}*\left(\frac{1}{\left(\frac{\mu_f}{\mu_{hnf}}\right)\left(\hat{\rho}_{hnf}\Big/\hat{\rho}_f\right)}\right)\\ &\left\{\frac{\partial\hat{\theta}}{\partial\xi}\frac{\partial\tilde{\psi}}{\partial\eta}-\frac{\partial\hat{\theta}}{\partial\eta}\frac{\partial\tilde{\psi}}{\partial\xi}\right\}+\mathrm{Pr}*\left(\frac{\mu_f}{\mu_{hnf}}\right)\left(\hat{\rho}_{hnf}\Big/\hat{\rho}_f\right)*\left(\frac{(\hat{\rho}c_p)_{hnf}}{(\hat{\rho}c_p)_f}\right)*\frac{Mn}{\left(\hat{\rho}_{hnf}\Big/\hat{\rho}_f\right)}\mathrm{Re}\\ &*\left(\frac{1}{\left(\frac{\mu_f}{\mu_{hnf}}\right)\left(\hat{\rho}_{hnf}\Big/\hat{\rho}_f\right)}\right)EcH(\varepsilon-\tilde{\psi})\left\{\frac{\partial H}{\partial\xi}\frac{\partial\tilde{\psi}}{\partial\eta}-\frac{\partial H}{\partial\eta}\frac{\partial\tilde{\psi}}{\partial\xi}\right\}\\ &+\mathrm{Pr}*\left(\hat{\rho}_{hnf}\Big/\hat{\rho}_f\right)\left(\frac{\mu_f}{\mu_{hnf}}\right)*\left(\frac{(\hat{\rho}c_p)_{hnf}}{(\hat{\rho}c_p)_f}\right)Ec\left\{\left(\frac{\partial^2\tilde{\psi}}{\partial\eta^2}-\frac{\partial^2\tilde{\psi}}{\partial\xi^2}\right)^2+4\left(\frac{\partial^2\tilde{\psi}}{\partial\xi\partial\eta}\right)^2\right\},\end{aligned} \tag{11}$$

Here, the dimensionless parameters u and v denote the velocities in the X and Y directions within the Cartesian coordinate system. $\hat{\theta}$ represents the temperature, C signifies the oxygen concentration, and N denotes the microorganism (bacteria) number density. Additionally, Ec, Pr, and Re correspond to the Eckert number, Prandtl number, and Reynolds number, respectively.

$$\begin{aligned}H_1(\xi,\eta)&=H_0\left\{\tanh A_1\left(\xi-\xi_1\right)-\tanh A_2\left(\xi-\xi_2\right)\right\},\\ H_2(\xi,\eta)&=H_0\left\{\tanh A_1\left(\xi-\xi_3\right)-\tanh A_2\left(\xi-\xi_4\right)\right\}\end{aligned} \tag{13}$$

In the strips defined by $\xi_1\le\xi\le\xi_2,\ \xi_3\le\xi\le\xi_4;\ 0\le\eta\le1$, respectively.

$$\text{Finally, } H\left(\xi,\eta\right)=H_1\left(\xi,\eta\right)+H_2\left(\xi,\eta\right) \tag{14}$$

We employ the stream-vorticity formulation, which adjusts Equations (1)-(4) using

$$\hat{u}=\frac{\partial\tilde{\psi}}{\partial\eta},\ \hat{v}=\frac{\partial\tilde{\psi}}{\partial\xi}\ \text{and}\ \left(\frac{\partial\hat{u}}{\partial\eta}-\frac{\partial\hat{v}}{\partial\xi}\right)=-\hat{\omega}\ \text{or}\ \left\{\left(\frac{\partial^2\tilde{\psi}}{\partial\xi^2}+\frac{\partial^2\tilde{\psi}}{\partial\eta^2}\right)=-\hat{\omega}\right\}. \tag{15}$$

Similarly, the non-dimensional boundary conditions are given as follows:

Left and Right Vertical Walls (Adiabatic):

$$\left.\begin{array}{l}\left(\frac{\partial\theta}{\partial\xi}\right)_{\xi=0}=0,\left(\frac{\partial\theta}{\partial\xi}\right)_{\xi=1}=0,\\ \hat{u}(0,\eta)=\hat{u}(1,\eta)=0,\\ \hat{v}(0,\eta)=\hat{v}(1,\eta)=0,\end{array}\right\}\quad 0\le\eta\le 1 \tag{16a}$$

Lower Horizontal Wall:

$$\left.\begin{array}{ll}\hat{u}(\xi,0)=0, & \hat{\theta}(\xi,0)=1,\\ \hat{v}(\xi,0)=0; & N(\xi,0)=0\end{array}\right\}\quad 0\le\xi\le 1. \tag{16b}$$

Upper Horizontal Wall:

$$\left.\begin{array}{l}\hat{u}(\xi,1)=-1,\\ \hat{v}(\xi,1)=0;\\ \hat{\theta}(\xi,1)=0,\end{array}\right\}\quad 0\le\xi\le 1 \tag{16c}$$

6.2 Key Physical Parameters

In the current work, the skin friction coefficient (CfRe) and the Nusselt number (Nu) are taken as the main performance indicators and are defined as follows:

$$\text{Nu}=\frac{\hat{q}L}{k_{hnf}\Delta T}\ \text{and}\ \text{CfRe}=\frac{2\tau}{\hat{\rho}_{hnf}v_0^{\,2}}$$

where,

$\tau=\tilde{\mu}_{hnf}\left(\frac{\partial\hat{U}}{\partial\eta}\right)\Big\vert_{\eta=0,L}$	shear stress	$\hat{q}=-k_{hnf}\left(\frac{\partial T}{\partial\eta}\right)\Big\vert_{\eta=0,L}$	heat flux

Incorporating dimensionless quantities gives rise to the following expressions:

$$\text{CfRe}=\left(\frac{\hat{\rho}_f}{\hat{\rho}_{hnf}}\right)\left(\frac{\mu_{hnf}}{\mu_f}\right)\frac{\partial\hat{u}}{\partial y},\ \text{and}\ N_u=\left(\frac{k_{hnf}}{k_f}\right)\frac{\partial\hat{\theta}}{\partial y}.$$

4. Numerical Scheme

The dimensionless governing equations (Eqs. (10)–(11)), together with the associated boundary conditions given in Eq. (16), are solved numerically using a pseudo-time marching technique, where the temporal term is treated as an iterative parameter to obtain the steady-state solution upon convergence. Further details of the numerical implementation can be found in [38]. **Fig. 2** illustrates the flow chart for the method employed.

5. Validity of the Numerical Method

The computed horizontal velocity profiles are compared with the published results of Asia et al. [39] for the cases of $\hat{\varphi}_1 = \hat{\varphi}_2 = 0$, Mn = 0, and a single moving lid driving the flow in the cavity to check the validity of the present numerical methodology. The comparison is made on three horizontal slices (y = 0.25, 0.5, 0.75). A good agreement is seen between the present numerical predictions and the previously reported results, as shown in **Fig. 3**, which confirms the reliability and accuracy of the numerical scheme used.

In addition, **Fig. 4** shows the grid-independence study by tracking the dependence of the computational results on the step size (distance between grid points). The findings show that the results converge smoothly as the step

size decreases and are free of numerical oscillations or instability. This is evidence of the stability and robustness of the numerical method. It also suggests that once a certain level of grid resolution is attained, the change in the results with increasing resolution is minimal, thus assuring us about the present calculations.

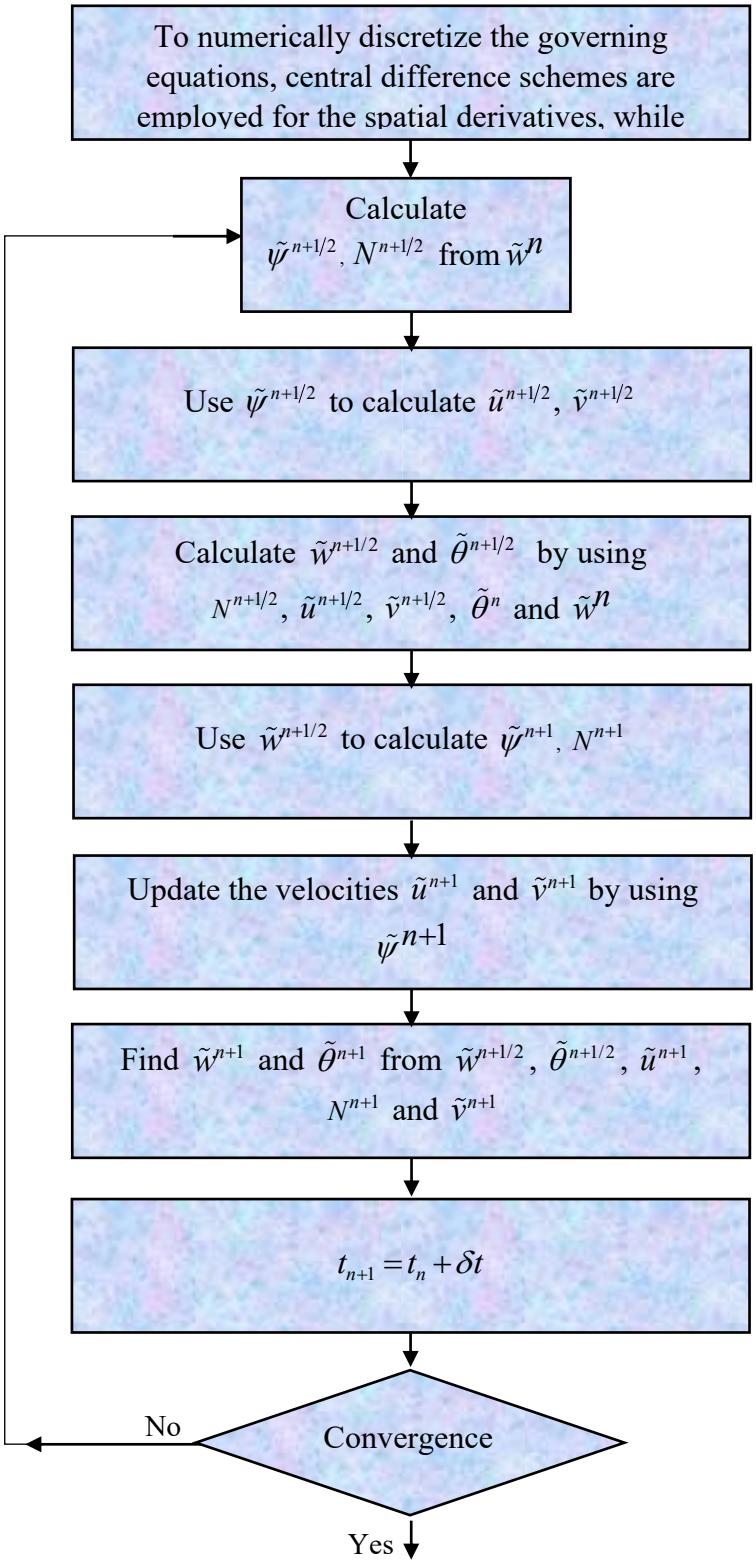

Fig. 2. Flow Diagram of the Pseudo-Transient Numerical Procedure

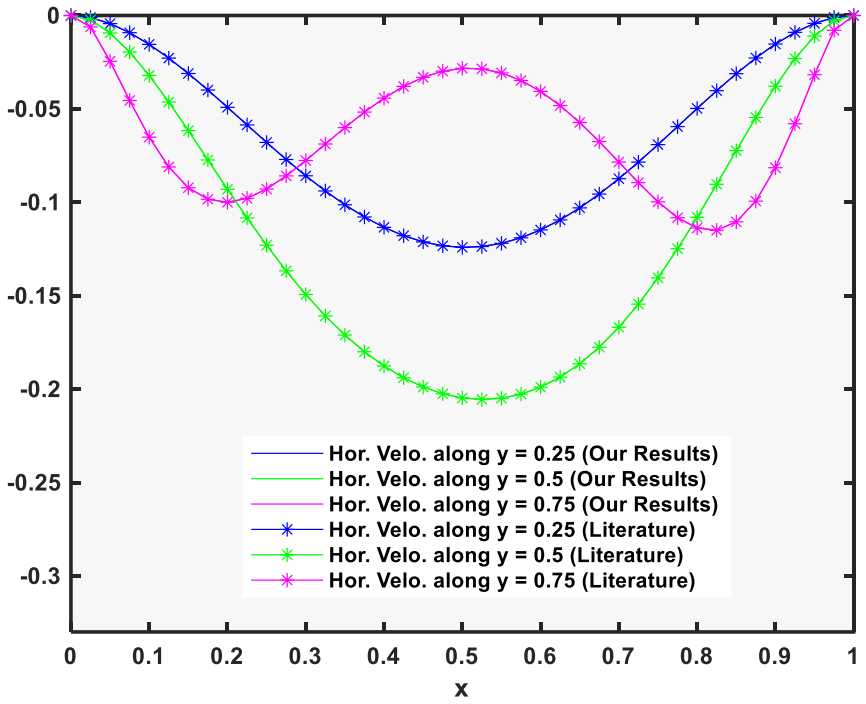

Fig. 3. Validation of the Present Numerical Results Through Comparison with the Analytical Solution Reported by Shih and Tan [40].

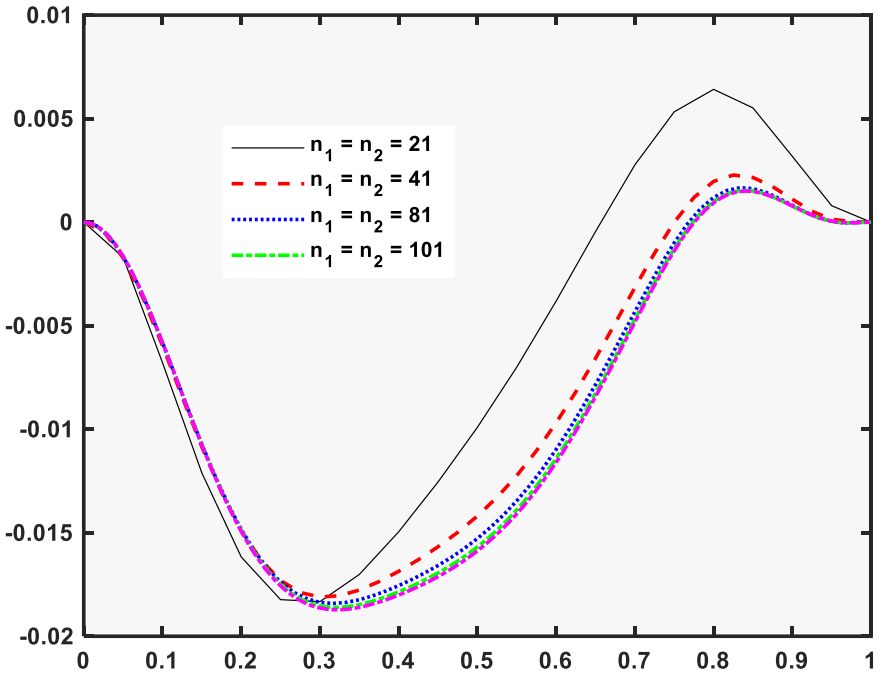

Fig. 4 Study of Mesh Sensitivity for a Normal Velocity Distribution

6. Results and Discussion

Here, we display the streamline, isotherm, and microrotation contours that are presented in the tables and figures. These images give a detailed picture of the fluid flow and heat distribution within a cavity. We have also developed similar surfaces, such as temperature distributions, microrotations and streamlines, to better understand the numerical findings. The tables show the values of the Nusselt number (Nu) and skin friction (CfRe) at the top and bottom horizontal walls. The Nusselt number quantifies the rate of heat transfer through the wall, while CfRe

indicates the shear stress exerted by the fluid on the wall. These findings apply to a situation where shear-driven flow is created inside an enclosure when the horizontal lids of the vertical enclosure move in a positive direction. Nevertheless, the enclosure's magnetic field is set up in strips, which are described as: $\xi_1 \le \xi \le \xi_2,\ \xi_3 \le \xi \le \xi_4;\ 0 \le \eta \le 1$, which produce areas at particular vertical cavity sections with almost uniform magnetic fields. This study examines several factors and their ranges, including the nanoparticle concentration. $\left(0 \le \hat{\varphi}_1, \hat{\varphi}_2 \le 0.10\right)$, the Reynolds number $\left(1 \le \mathrm{Re} \le 100\right)$, the magnetic number $\left(0 \le \mathrm{Mn} \le 200\right)$, signifying the microrotation parameter, and the flow's magnetic field strength $\left(0 \le \mathrm{C} \le 10\right)$.

6.1 Role of Magnetic Strips

The effect of the magnetic parameter (Mn) on the inside streamline and isotherm distribution in the cavity filled with the hybrid nanofluid is shown in **Fig. 5**. Without a magnetic field (Mn = 0), the flow is dominated by a single vortex in most of the enclosure, and the relative smoothness and uniform distribution of the isotherms. When the magnetic parameter is increased, the Lorentz force caused by the localized magnetic strips greatly influences the flow structure and thermal field. The vortices are clearly seen to be mainly generated around the two magnetic strips, clearly showing the strong influence of the localized magnetic field on the vortex generation process near the magnetized regions. As the flow increases (Mn), more secondary vortices form and the streamline patterns elongate vertically around the strips. Concurrently, the main circulation in the cavity is more compressed in the vertical direction as a result of the increased magnetic suppression effect. The isotherms are also more distorted and vertically compressed, especially in the region of the magnetic strips, indicating better mixing of the fluid and stronger thermal interaction between the hot bottom wall and the cold moving upper lid. For larger magnetic strengths (Mn = 60 and 200), several recirculation regions occur near the strips and cavity corners, and the thermal contours appear more and more non-uniform due to the enhanced interaction between the vortices and the local thermal transport. These findings validate the localized magnetic field as a valuable tool to manipulate and control the vortex dynamics, suppress the motion of the fluid, and alter the heat transfer characteristics within the cavity.

6.2 Consequences of Reynolds Number

The Reynolds number (Re) effects on the streamline and isotherm distribution inside the cavity containing the hybrid nanofluid are shown in **Fig. 6**. The results show that the overall flow structure and thermal field are moderately affected by increasing Reynolds number, but more affected by the magnetic parameter effects. The flow is primarily controlled by the primary circulation cell formed by the flow of the top lid at lower Reynolds numbers, and the isotherms are relatively smooth and well-spaced out. With increasing Reynolds number, this

fluid circulation inside the cavity becomes slightly stronger because of the increase in inertial forces. This is an increase in inertia which amplifies the rotation of the fluid and causes a slight elongation of the vortex structures within the flow domain. Overall, the streamline topology is still very similar, only slightly modified, showing that the local magnetic field still exerts the dominant influence on the flow. The isotherm patterns also exhibit very little change with increasing Reynolds number. A slight improvement in thermal mixing can be seen near the moving lid and magnetic strips, which slightly improves the convective heat transfer in the cavity. However, the temperature contours retain the overall shape, indicating that the thermal field is less sensitive to the variation of Reynolds number in the range of interest.

6.3 Impact of Localization

For various widths of the localized magnetic strips (L) in the cavity, the streamline and isotherm distributions are shown in **Fig. 7**. Two strips of magnets are placed vertically in the regions $\left(0.2 - L < \xi < 0.3 + L,\ 0.7 - L < \xi < 0.8 + L,\ 0 < \eta < 1\right)$ and $\left(0.2 - L < \eta < 0.3 + L,\ 0.7 - L < \eta < 0.8 + L,\ 0 < \xi < 1\right)$ to create the magnetic field. The results clearly show

Mn	Streamlines	Isotherms

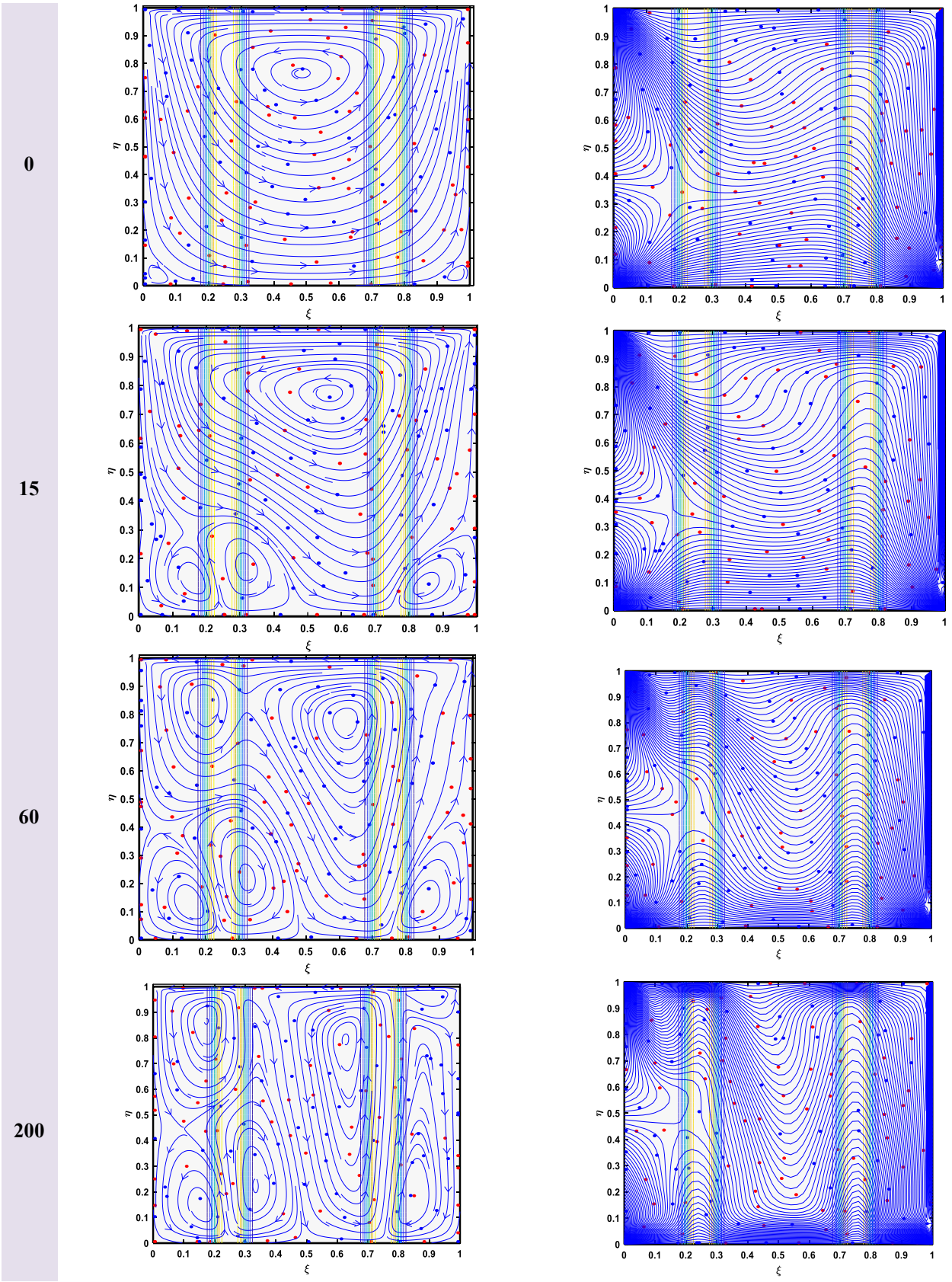

Fig. 5. Visualization of Flow Patterns through Streamlines and Isotherms at Various Mn.

Re	Streamlines	Isotherms

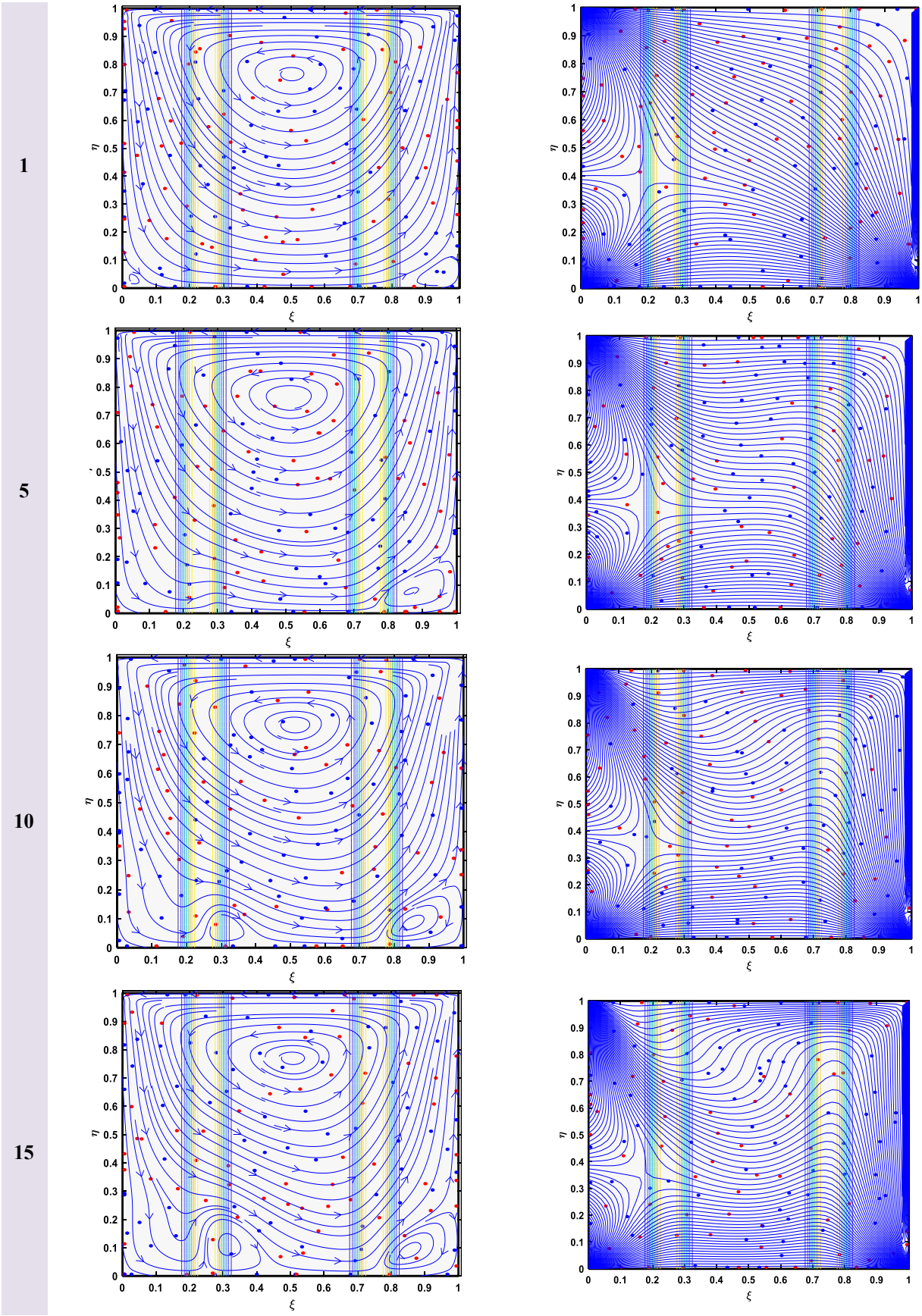

Fig. 6. Visualization of Flow Patterns through Streamlines and Isotherms at Various Re.

that the vortex dynamics and thermal behavior of the hybrid nanofluid flow are significantly affected by the extension of the magnetic strips.

It is found that the vortices are primarily stronger formed around the magnetic strips, which supports the idea that the localized Lorentz force is the primary control of the flow structure near the magnetic strips. The magnetic strips are aligned vertically, which makes the vortical structures also vertically elongated. The streamlines are very distinct between the strips, and many vortices are evident around the two magnetic regions at smaller strip widths (L = 0.0). The wider the strip, the more magnetic influence it has on a larger portion of the cavity, and the more the neighboring vortices interact with each other, the more magnetic influence is generated on them, and they tend to merge. For intermediate strip widths (L = 0.05 and 0.10), the interaction between the vortices becomes more noticeable, and the dividing region between the two circulation zones starts to weaken. This is because the length of the magnetic regions decreases the unmagnetized spacing between the strips, thereby increasing the coupling between the localized recirculation cells. As the strip width increases (L = 0.15 and 0.199), the vortices almost join to a single dominant circulation structure that covers most of the cavity with only small secondary vortices located near the lower corners. This can also be seen from the isotherm distributions. The temperature contours are more and more distorted and stretched vertically as the magnetic strips grow larger as a result of the increased fluid mixing caused by the interaction of the vortices. The improved circulation helps to exchange the heat energy between the heated lower wall and the cooled upper moving lid, resulting in a stronger convective heat transfer inside the enclosure.

6.4 Effects of Governing Parameters on Heat Transfer Rate and Wall Shear Stress

The effects of the magnetic parameter (Mn) and Reynolds number (Re) on the Nusselt number (Nu) and skin friction coefficient (CfRe) along the moving wall of the cavity are shown in **Fig. 8**. The trends in both (Mn) and (Re) are similar in (CfRe) but the effect of (Re) on the Nusselt number is significantly larger than that of (Mn). An increase in either parameter increases the fluctuations of both heat transfer and wall shear characteristics. When the magnetic field is uniformly distributed over the whole cavity, the parameter (L) has almost a linear response. However, if the magnetic field is confined to localized areas, the distribution of (Nu) and (CfRe) will be significantly changed, suggesting the presence of vortices with different rotational behaviors. The greatest difference is found at (L=0.10), where both the thermal transport and shear stress characteristics are strongly affected. Furthermore, the volume fractions of nanoparticles ($\hat{\varphi}_1, \hat{\varphi}_2$) have different effects on the thermal and hydrodynamic properties. The parameter ($\hat{\varphi}_2$) has a larger influence on the skin friction coefficient, while the parameter ($\hat{\varphi}_1$) has a more significant effect on the enhancement of the Nusselt number.

6.5 Influence of Governing Parameters on Thermo-Physical Quantities

Tables 1 and **2** show the average Nusselt number (Nu) and skin friction coefficient (CfRe) along the moving wall of the cavity for the effect of the magnetic parameter (Mn) and Reynolds number (Re), respectively. The outcomes reveal that both parameters significantly influence the thermo-hydrodynamic parameters of the hybrid nanofluid flow, but the influence is of various magnitudes and physical behavior. Generally, as either Mn or Re is increased, the circulation of the flow is enhanced, and the wall shear distribution in the cavity changes. It is noticed from **Table 1** that the average Nusselt number increases by about 7.5%. Simultaneously, the skin friction coefficient increases by nearly 253%. It is observed that this behavior is attributed to the formation of higher Lorentz forces in the localized magnetic field, which leads to the creation of more vortical structures in the conducting hybrid nanofluid and increases the fluid mixing around the magnetic strips. The improved mixing results in more efficient transfer of the thermal energy from the heated lower wall to the cooled moving upper wall, thus boosting the heat transfer rate. Furthermore, as the magnetic interaction gets stronger, the resistance to the motion of the fluid near the walls increases, resulting in a considerable increase in the wall shear stress and skin friction.

It is observed from **Table 2** that the Reynolds number has a significant effect on the enhancement of the heat transfer coefficient as compared to the magnetic parameter. The Reynolds number increases from (Re=1) to (Re=100), the average Nusselt number increases from (0.8272) to (3.7576), which is an increase of about (354%). Likewise, the skin friction coefficient rises from (0.7919) to (4.5826), which represents an increase of almost (479%). Increasing the Reynolds number enhances the inertial forces within the cavity and the lid-driven circulation. The turbulent flow leads to strong convection currents and this increases the mixing of hot and cold fluid layers, leading to a significant increase in convective heat transfer. The increased fluid motion, however,

also raises the velocity gradients close to the cavity walls, thus directly affecting the wall shear stress and the frictional resistance.

L	Streamlines	Isotherms
0	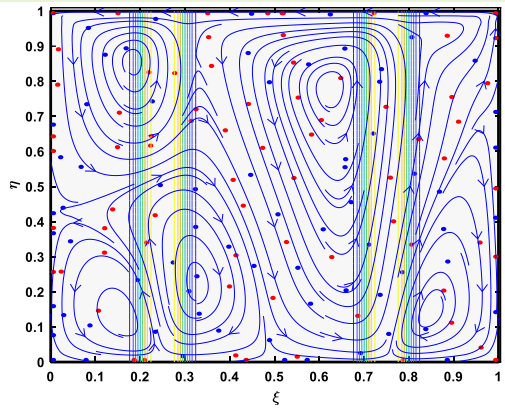	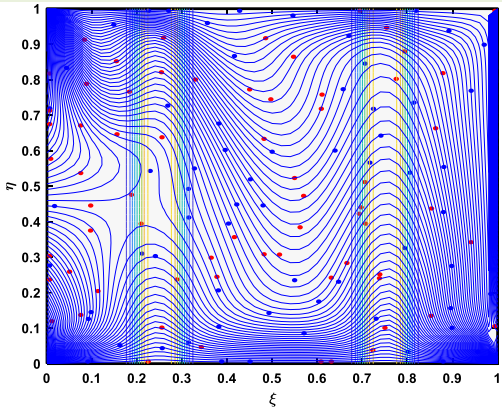
0.05	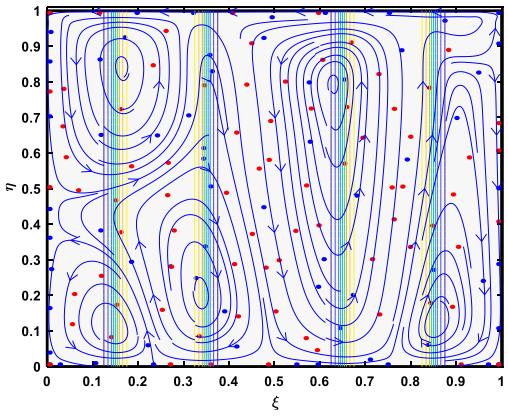	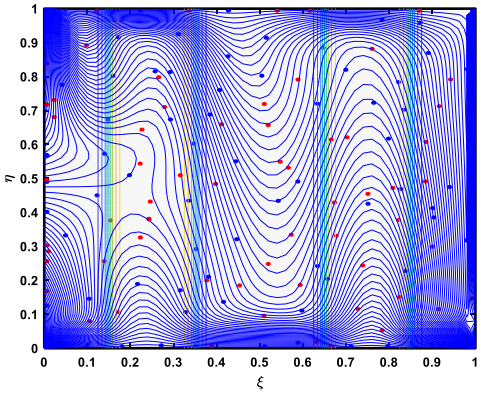
0.10	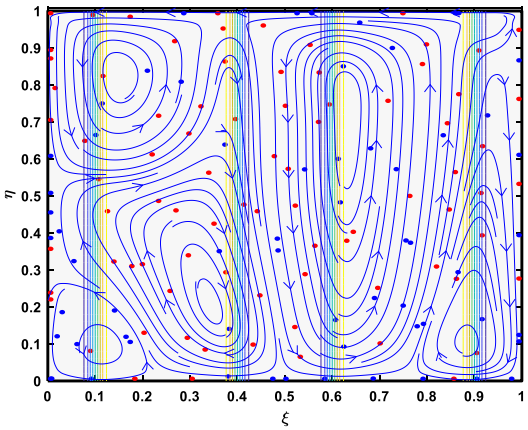	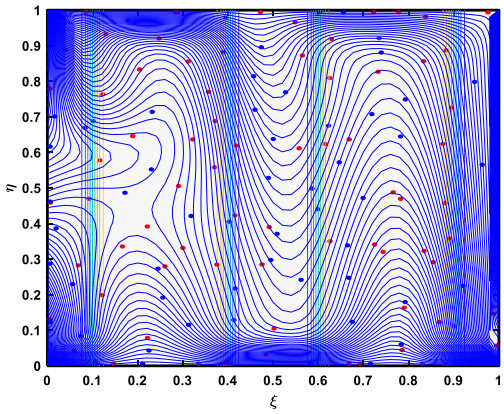
0.15	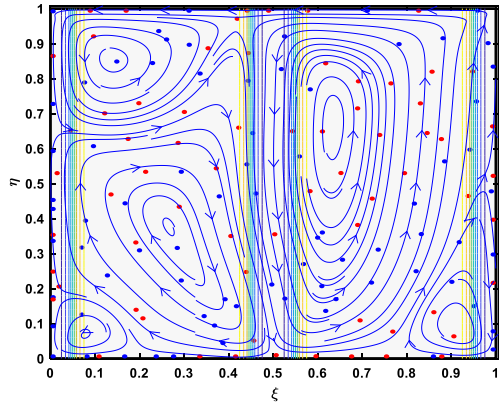	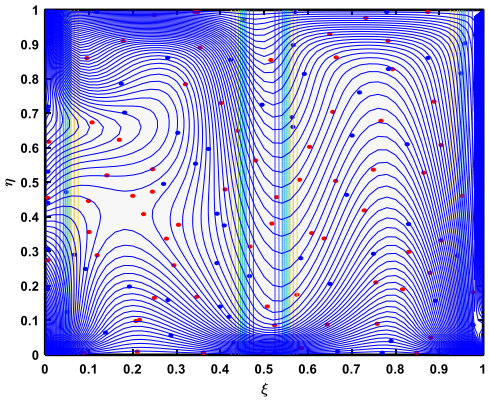

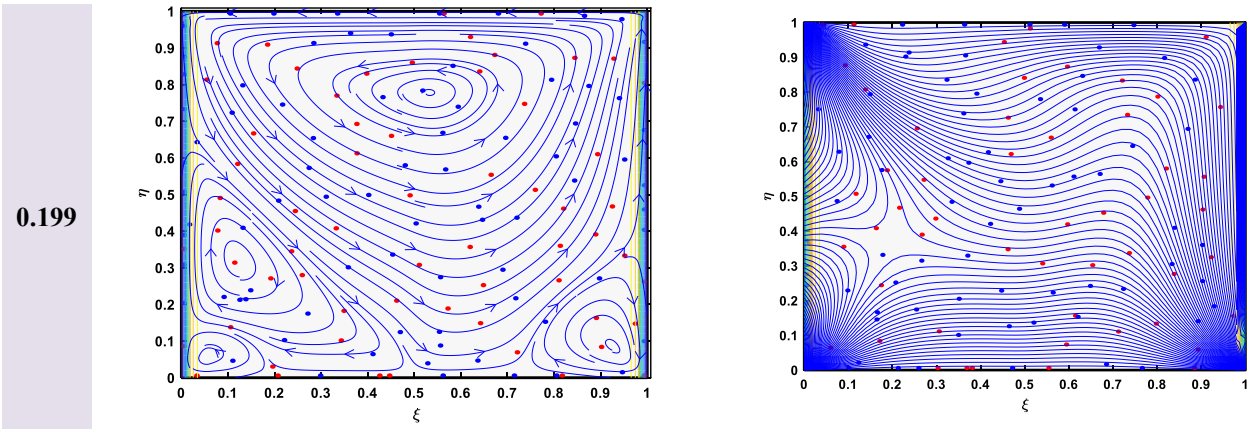

Fig. 7. Visualization of Flow Patterns through Streamlines and Isotherms at Various Widths of Magnetic Field (L).

The variation of the Nusselt number and the skin friction coefficient with the geometric parameter (L) associated with the width of the localized magnetic strips is summarized in **Table 3**. The results show that the thermal and hydrodynamic responses are very sensitive to the magnetic strip extension. The Nusselt number increases from 2.3216 to 3.0186 as L increases from 0.00 to 0.10, which is an approximate (30%) enhancement. Likewise, the skin friction coefficient increases by almost 95%. This enhancement is due to an increase in the magnetic strips, which increases the magnetically active area, and thus increases the interaction of the vortex and the mixing of the fluid inside the cavity. But, as the magnetic strips are further extended to L=0.20, the Nusselt number reduces to 2.1872, and the skin friction coefficient reduces significantly to 1.6211. The decrease implies that magnetic-field expansion causes a decrease in the local vortex interaction, which in turn decreases the intensity of the recirculation zones that enhance the thermal effect.

Tables 4 show the thermal and hydrodynamic performance of the hybrid nanofluid at various volume fractions of the nanoparticles. From the concentration level of up to 20%, the average Nusselt number (Nu) improves by 114%. The skin friction coefficient also increases by 67% enhancement. This significant improvement is attributed mainly to the high thermal conductivity of silver nanoparticles, which increases the thermal diffusion and energy transport in the cavity. The increase in the concentration of the nanoparticles, however, causes the effective viscosity of the hybrid nanofluid to increase as well, causing an increase in wall shear stress.

On the other hand, **Table 5** suggests that the average Nusselt number (Nu) increases by about 40%. The skin friction coefficient for silver nanoparticles decreases by 32% approximately, unlike the silver nanoparticles. This behavior indicates that iron oxide nanoparticles have a better heat transfer ability and less viscous effect on fluid flow, possibly related to magnetic interaction and a weaker viscous effect of the nanoparticles on fluid flow compared to the other particles.

6.6 Comparative Evaluation of the Thermal Performance of Different Nanomaterials

Two key points are emphasized in **Fig. 9,** first, it is observed that the average Nusselt number (Nu) increases almost linearly with the nanoparticle volume concentration. Second, the hybrid nanofluid of Cu- Fe_3O_4 nanoparticles has a greater average Nusselt number than the conventional Ag and Fe_3O_4 nanoparticles-based nanofluids.

6.7 Impact of Magnetic Field Intensity

Equation (9b) includes the parameters ξ_1, ξ_2, ξ_3 and ξ_4, which characterize the locations of the two magnetic fields associated with a pair of vertical strips defined within the regions $\xi_1 \leq \xi \leq \xi_2, \xi_3 \leq \xi \leq \xi_4$ and $0 \leq \eta \leq 1$. The values A1 and A2 are the magnetic field intensity. As shown in **Fig. 10**, the sensitivity of the heat transfer enhancement is more noticeable for lower values of the parameters A1 and A2.

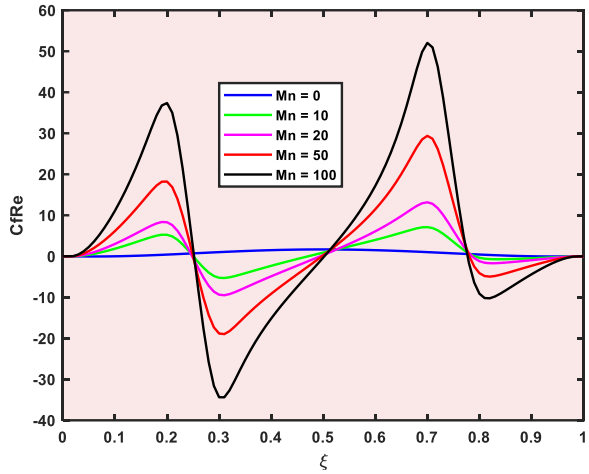
Mn = 0
Mn = 10
Mn = 20
Mn = 50
Mn = 100
CfRe
ξ

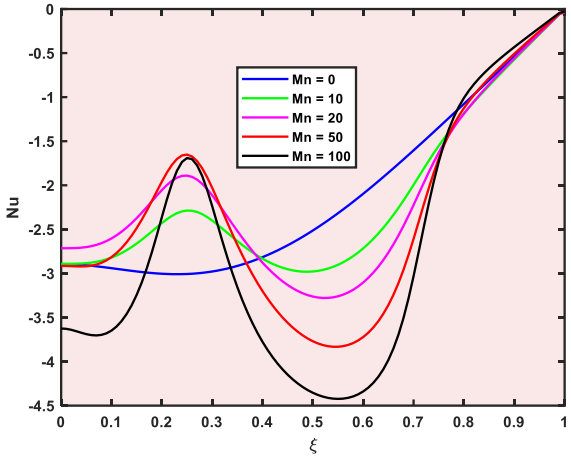
Mn = 0
Mn = 10
Mn = 20
Mn = 50
Mn = 100
Nu
ξ

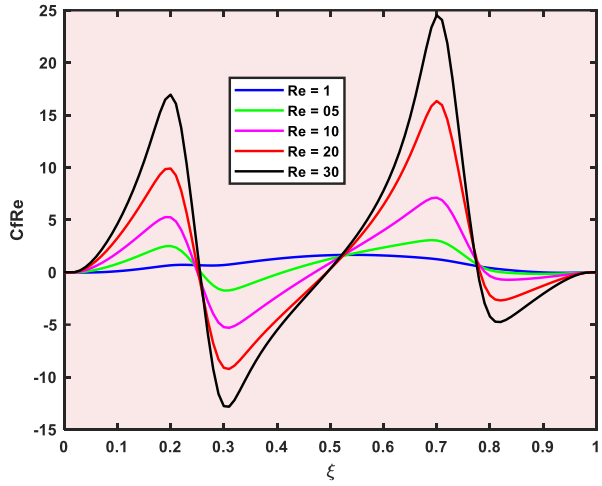
Re = 1
Re = 05
Re = 10
Re = 20
Re = 30
CfRe
ξ

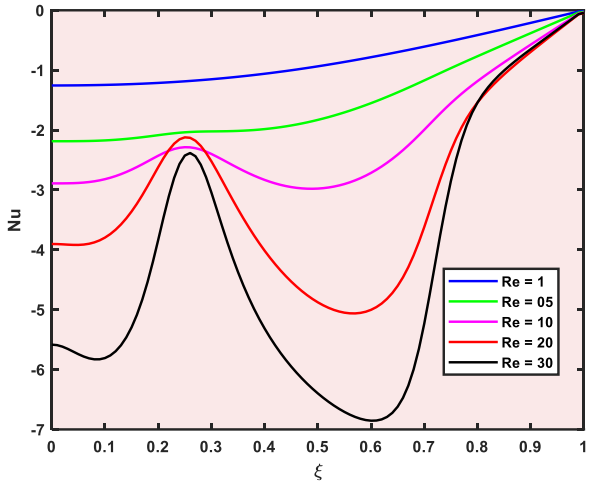
Re = 1
Re = 05
Re = 10
Re = 20
Re = 30
Nu
ξ

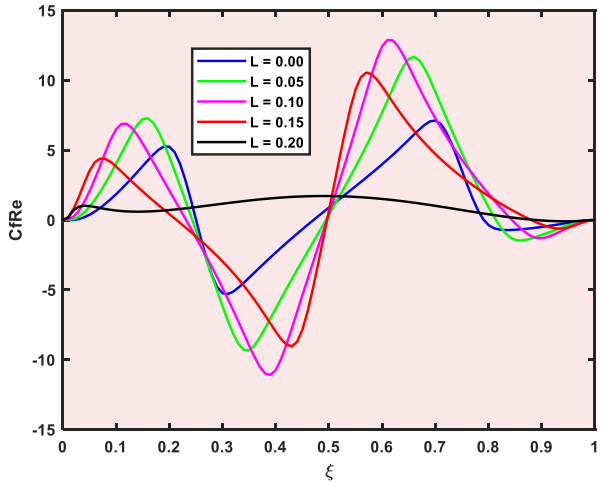
L = 0.00
L = 0.05
L = 0.10
L = 0.15
L = 0.20
CfRe
ξ

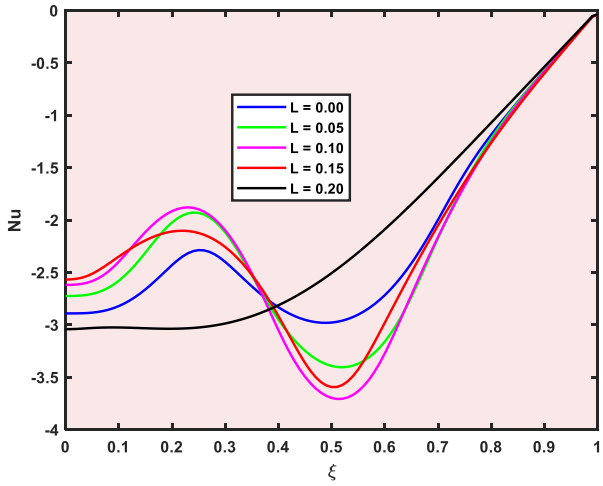
L = 0.00
L = 0.05
L = 0.10
L = 0.15
L = 0.20
Nu
ξ

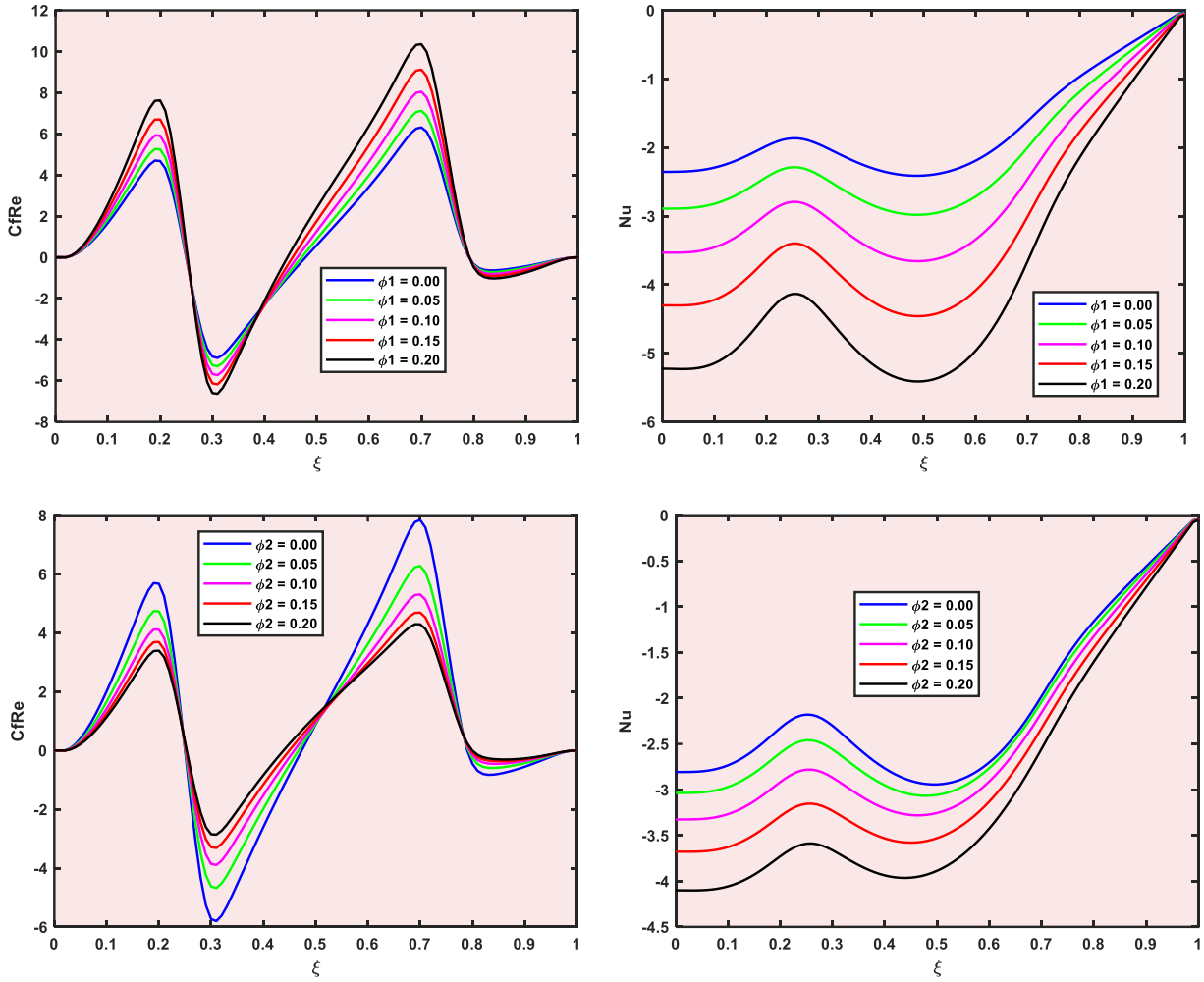

Fig. 8. Variations in Skin Friction (CfRe) and Nusselt Number (Nu) Across Different Parameters

6.8 Impact of Localized Lorentz Force

Impact of nanoparticle volume fraction on the average heat transfer (Nu) for various widths of the localized magnetic strips (L) is shown in **Fig. 11**. The results show that the average Nusselt number is almost linearly proportional to the concentration of nanoparticles, which means that the thermal transport property of the working fluid is consistently improved by the addition of nanoparticles. It is also clear that the effect of the concentration of the nanoparticles is almost independent of the magnetic strip width, as all the curves show a similar linear trend for different values of L. However, as the width of the strip is increased, the overall magnitude of the Nusselt number is increased, indicating that a wider magnetic-field region is beneficial to the convective heat transfer in the cavity. The magnetic strips are defined by the regions $\xi_1 - L \leq x \leq \xi_2 + L, \xi_3 - L \leq x \leq \xi_4 + L \text{with} 0 \leq \eta \leq 1$.

Table 1. Behavior of Skin Friction Coefficient (CfRe), and Nusselt Number (Nu) under Different Magnetic Interaction Parameter (Mn)

Mn	|Nu|	|CfRe|
00	2.1059	0.7516
20	2.1222	0.9105
50	2.1385	1.0772
70	2.1872	1.6211
100	2.2643	2.6532

Table 2. Behavior of Skin Friction Coefficient (CfRe), and Nusselt Number (Nu) under Different Reynolds Numbers (Re)

Re	|Nu|	|CfRe|
01	0.8272	0.7919
20	2.1872	1.6211
50	2.6563	2.2908
70	3.0525	3.0516
100	3.7576	4.5826

Table 3. Behavior of Skin Friction Coefficient (CfRe), and Nusselt Number (Nu) under L

L	|Nu|	|CfRe|
0.00	2.3216	2.9742
0.05	2.8279	5.3309
0.10	3.0186	5.7955
0.15	2.7006	3.4157
0.20	2.1872	1.6211

Table 4. Behavior of Skin Friction Coefficient (CfRe), and Nusselt Number (Nu) under Different Nanoparticle Volume Fraction ($\hat{\varphi}_1$)

$\hat{\varphi}_1$*(Silver)*	|Nu|	|CfRe|
0.00	1.7986	1.4458
0.05	2.1872	1.6211
0.10	2.6470	1.8323
0.15	3.1947	2.0913
0.20	3.8527	2.4141

Table 5. Behavior of Skin Friction Coefficient (CfRe), and Nusselt Number (Nu) under Different Nanoparticle Volume Fraction ($\hat{\varphi}_2$)

$\hat{\varphi}_2$*(Iron Oxide)*	|Nu|	|CfRe|
0.00	2.1359	1.7408
0.05	2.2786	1.4825
0.10	2.4688	1.3273
0.15	2.7082	1.2355
0.20	3.0022	1.1876

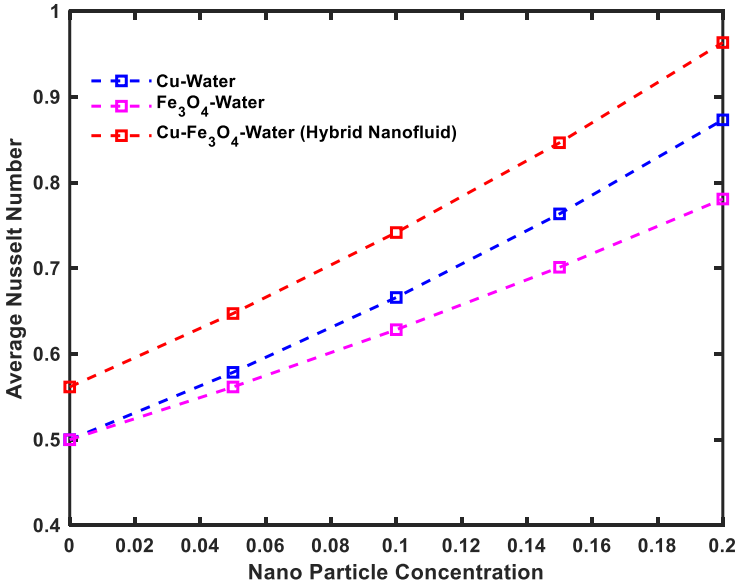

Fig. 9. Comparative Assessment of Thermal Performance Between Individual Nanoparticles and Hybrid Nanofluids

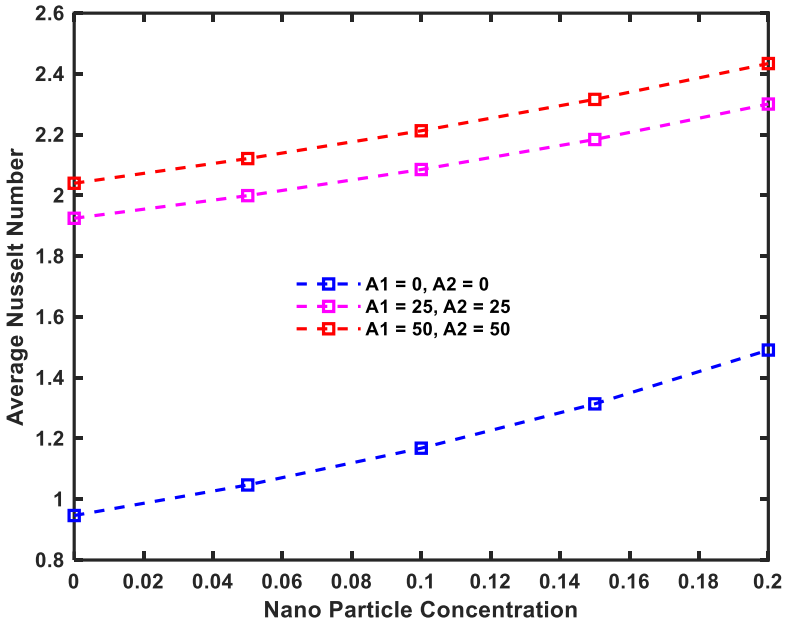

Fig. 10. Effect of Magnetic Field Intensity Parameters A_1 and A_2 on the Average Nusselt Number

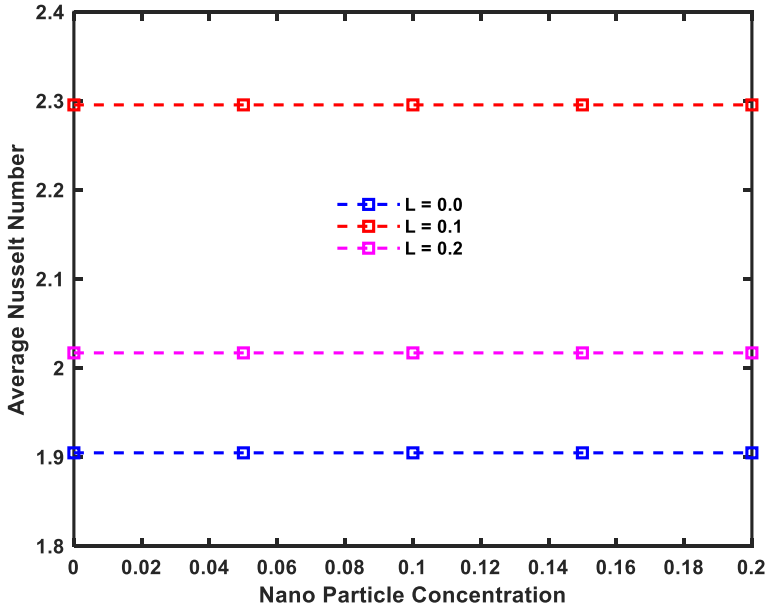

Fig. 11. Influence of Localized Magnetic Strip Width on the Average Nusselt Number

7. Concluding Remarks

The present study numerically examines the effects of localized magnetic fields on vortex formation and heat transfer enhancement within a lid-driven cavity containing Ag–Fe_3O_4/water hybrid nanofluid by employing the Alternating Direction Implicit (ADI) method. A detailed analysis is carried out to explore the impacts of the magnetic interaction parameter (Mn), Reynolds number (Re), magnetic strip width (L), and nanoparticle volume fraction on the flow behavior and thermal performance of the system.

The results demonstrated that the localized magnetic strips significantly modified the streamline structure and thermal field through Lorentz-force-induced vortex generation. Increasing the magnetic interaction parameter from Mn=0 to Mn=100 enhanced the average Nusselt number from 2.1059 to 2.2643, corresponding to an improvement of approximately 7.5%, while the skin friction coefficient increased by nearly 253%. This enhancement was mainly attributed to the stronger localized recirculation zones and improved thermal mixing

generated near the magnetic strips. The Reynolds number exhibited the strongest influence on thermo-hydrodynamic performance. As the Reynolds number increased from Re=1 to Re=100, the average Nusselt number increased from 0.8272 to 3.7576, representing an enhancement of approximately 354%, whereas the skin friction coefficient increased by nearly 479%. The stronger inertial forces intensified the circulation inside the cavity and substantially improved convective heat transfer between the heated lower wall and the cooled upper moving lid. The width of the localized magnetic strips also played a critical role in controlling vortex interaction and heat transfer performance. Increasing the strip width from L=0.00 to L=0.10 enhanced the average Nusselt number by approximately 30% and increased the skin friction coefficient by nearly 95%. However, further enlargement of the magnetic strips weakened the localized vortex interaction and reduced the thermal enhancement due to excessive magnetic suppression of the fluid motion. The nanoparticle concentration considerably improved the thermal behavior of the hybrid nanofluid. Increasing the silver nanoparticle volume fraction from 0% to 20% enhanced the average Nusselt number by approximately 114%, accompanied by nearly 67% enhancement in the skin friction coefficient due to increased viscosity effects. Similarly, increasing the Fe_3O_4 nanoparticle concentration improved the average Nusselt number by approximately 40%, while reducing the skin friction coefficient by nearly 32%, indicating better thermal enhancement with comparatively lower viscous resistance.

Overall, the study confirms that localized magnetic fields provide an efficient mechanism for manipulating vortex dynamics, controlling fluid circulation, and enhancing convective heat transfer inside hybrid nanofluid-filled enclosures. The proposed configuration may be useful in the design of advanced thermal management systems, cooling technologies, electronic devices, and magnetically controlled heat transfer applications.

Funding (Acknowledgments)

The authors extend their appreciation to Prince Sattam bin Abdulaziz University for funding this research work through the project number (PSAU/2026-01-44901).

References

[1] A. Alsabery, A. J. Chamkha, H. Saleh, I. Hashim, Heatline visualization of conjugate natural convection in a square cavity filled with nanofluid with sinusoidal temperature variations on both horizontal walls, *International Journal of Heat and Mass Transfer,* Vol. 100, pp. 835-850, 2016.

[2] F. Selimefendigil, H. F. Öztop, Conjugate natural convection in a cavity with a conductive partition and filled with different nanofluids on different sides of the partition, *Journal of Molecular Liquids,* Vol. 216, pp. 67-77, 2016.

[3] F. Garoosi, L. Jahanshaloo, M. M. Rashidi, A. Badakhsh, M. E. Ali, Numerical simulation of natural convection of the nanofluid in heat exchangers using a Buongiorno model, *Applied Mathematics and Computation,* Vol. 254, pp. 183-203, 2015.

[4] M. Sheikholeslami, T. Hayat, A. Alsaedi, MHD free convection of Al2O3–water nanofluid considering thermal radiation: a numerical study, *International Journal of Heat and Mass Transfer,* Vol. 96, pp. 513-524, 2016.

[5] D. Pal, G. Mandal, K. Vajravelu, Flow and heat transfer of nanofluids at a stagnation point flow over a stretching/shrinking surface in a porous medium with thermal radiation, *Applied Mathematics and Computation,* Vol. 238, pp. 208-224, 2014.

[6] S. A. Shehzad, T. Hayat, A. Alsaedi, M. A. Obid, Nonlinear thermal radiation in three-dimensional flow of Jeffrey nanofluid: a model for solar energy, *Applied Mathematics and Computation,* Vol. 248, pp. 273-286, 2014.

[7] M. Sheikholeslami, D. Ganji, Nanofluid convective heat transfer using semi analytical and numerical approaches: a review, *Journal of the Taiwan Institute of Chemical Engineers,* Vol. 65, pp. 43-77, 2016.

[8] M. Ayub, T. Abbas, M. Bhatti, Inspiration of slip effects on electromagnetohydrodynamics (EMHD) nanofluid flow through a horizontal Riga plate, *The European Physical Journal Plus,* Vol. 131, No. 6, pp. 193, 2016.

[9] N. Shehzad, A. Zeeshan, R. Ellahi, K. Vafai, Convective heat transfer of nanofluid in a wavy channel: Buongiorno's mathematical model, *Journal of Molecular Liquids,* Vol. 222, pp. 446-455, 2016.

[10] M. M. Bhatti, T. Abbas, M. M. Rashidi, M. E.-S. Ali, Z. Yang, Entropy generation on MHD Eyring–Powell nanofluid through a permeable stretching surface, *Entropy,* Vol. 18, No. 6, pp. 224, 2016.

[11] M. Sheikholeslami, H. B. Rokni, Nanofluid two phase model analysis in existence of induced magnetic field, *International Journal of Heat and Mass Transfer,* Vol. 107, pp. 288-299, 2017.

[12] M. Sheikholeslami, D. Ganji, Nanofluid hydrothermal behavior in existence of Lorentz forces considering Joule heating effect, *Journal of Molecular Liquids,* Vol. 224, pp. 526-537, 2016.

[13] S. Marzougui, F. Mebarek-Oudina, M. Magherbi, A. Mchirgui, Entropy generation and heat transport of Cu–water nanoliquid in porous lid-driven cavity through magnetic field, *International Journal of Numerical Methods for Heat & Fluid Flow,* Vol. 32, No. 6, pp. 2047-2069, 2022.

[14] Z. Korei, S. Benissaad, F. Berrahil, A. Filali, MHD mixed convection and irreversibility analysis of hybrid nanofluids in a partially heated lid-driven cavity chamfered from the bottom side, *International Communications in Heat and Mass Transfer,* Vol. 132, pp. 105895, 2022.

[15] A. K. Prasad, J. R. Koseff, Combined forced and natural convection heat transfer in a deep lid-driven cavity flow, *International Journal of Heat and Fluid Flow,* Vol. 17, No. 5, pp. 460-467, 1996.

[16] W.-J. Luo, R.-J. Yang, Multiple fluid flow and heat transfer solutions in a two-sided lid-driven cavity, *International journal of heat and mass transfer,* Vol. 50, No. 11-12, pp. 2394-2405, 2007.

[17] B. John, X.-J. Gu, D. R. Emerson, Investigation of heat and mass transfer in a lid-driven cavity under nonequilibrium flow conditions, *Numerical Heat Transfer, Part B: Fundamentals,* Vol. 58, No. 5, pp. 287-303, 2010.

[18] M. Moallemi, K. Jang, Prandtl number effects on laminar mixed convection heat transfer in a lid-driven cavity, *International Journal of Heat and Mass Transfer,* Vol. 35, No. 8, pp. 1881-1892, 1992.

[19] K. Khanafer, Comparison of flow and heat transfer characteristics in a lid-driven cavity between flexible and modified geometry of a heated bottom wall, *International Journal of Heat and Mass Transfer,* Vol. 78, pp. 1032-1041, 2014.

[20] D. Chatterjee, S. K. Gupta, B. Mondal, Mixed convective transport in a lid-driven cavity containing a nanofluid and a rotating circular cylinder at the center, *International Communications in Heat and Mass Transfer,* Vol. 56, pp. 71-78, 2014.

[21] R. Roslan, H. Saleh, I. Hashim, Effect of rotating cylinder on heat transfer in a square enclosure filled with nanofluids, *International Journal of Heat and Mass Transfer,* Vol. 55, No. 23-24, pp. 7247-7256, 2012.

[22] V. Costa, A. Raimundo, Steady mixed convection in a differentially heated square enclosure with an active rotating circular cylinder, *International Journal of Heat and Mass Transfer,* Vol. 53, No. 5-6, pp. 1208-1219, 2010.

[23] M. Mahmoodi, S. M. Sebdani, Natural convection in a square cavity containing a nanofluid and an adiabatic square block at the center, *Superlattices and Microstructures,* Vol. 52, No. 2, pp. 261-275, 2012.

[24] S. Saedodin, M. Biglari, M. H. Esfe, M. J. Noroozi, Mixed convection heat transfer performance in a ventilated inclined cavity containing heated blocks: effect of dispersing Al2O3 in water and aspect ratio of the block, *Journal of Computational and Theoretical Nanoscience,* Vol. 10, No. 11, pp. 2663-2675, 2013.

[25] A. K. Kareem, S. Gao, Computational study of unsteady mixed convection heat transfer of nanofluids in a 3D closed lid-driven cavity, *International Communications in Heat and Mass Transfer,* Vol. 82, pp. 125-138, 2017.

[26] P. Verma, M. K. Das, Vortex structure and control in a lid-driven cavity with magnetic field, *Physics of Fluids,* Vol. 36, No. 12, 2024.

[27] M. U. Mahmuda Maya, M. N. Alam, A. Refaie Ali, Influence of magnetic field on MHD mixed convection in lid-driven cavity with heated wavy bottom surface, *Scientific Reports,* Vol. 13, No. 1, pp. 18959, 2023.

[28] A. Maneengam, T. Bouzennada, A. Abderrahmane, K. Guedri, W. Weera, O. Younis, B. Bouallegue, Numerical study of lid-driven hybrid nanofluid flow in a corrugated porous cavity in the presence of magnetic field, *Nanomaterials,* Vol. 12, No. 14, pp. 2390, 2022.

[29] M. J. Hasan, A. Azad, R. Hossain, M. Rahman, M. Karim, Analysis of mixed convection under radiation and magnetohydrodynamics utilizing Kerosene-CNT nanofluid in a lid-driven cavity, *International Journal of Thermofluids,* Vol. 21, pp. 100528, 2024.

[30] S. Hussain, A. M. Aly, H. F. Öztop, Magneto-bioconvection flow of hybrid nanofluid in the presence of oxytactic bacteria in a lid-driven cavity with a streamlined obstacle, *International Communications in Heat and Mass Transfer,* Vol. 134, pp. 106029, 2022.

[31] K. Herouz, H. Laidoudi, A. Aissa, A. Mourad, K. Guedri, M. Oreijah, O. Younis, Analysis of nano-encapsulated phase change material confined in a double lid-driven hexagonal porous chamber with an obstacle under magnetic field, *Journal of Energy Storage,* Vol. 61, pp. 106736, 2023.

[32] F. Talebi, A. H. Mahmoudi, M. Shahi, Numerical study of mixed convection flows in a square lid-driven cavity utilizing nanofluid, *International Communications in Heat and Mass Transfer,* Vol. 37, No. 1, pp. 79-90, 2010.

[33] N. Acharya, S. Maity, P. K. Kundu, Framing the hydrothermal features of magnetized TiO2–CoFe2O4 water-based steady hybrid nanofluid flow over a radiative revolving disk, *Multidiscipline Modeling in Materials and Structures*, 2019.

[34] S. Ahmad, K. Ali, M. Ashraf, MHD flow of Cu-Al 2 O 3/water hybrid nanofluid through a porous media, *Journal of Porous Media,* Vol. 24, No. 7, 2021.

[35] S. Ahmad, K. Ali, T. Sajid, U. Bashir, F. Lafta Rashid, R. Kumar, M. R. Ali, A. S. Hendy, A. Darvesh, A novel vortex dynamics for micropolar fluid flow in a lid-driven cavity with magnetic field localization – A computational approach, *Ain Shams Engineering Journal*, pp. 102448, 2023/08/28/, 2023.

[36] S. Ahmad, K. Ali, A. Ayub, U. Bashir, F. L. Rashid, Y. Aryanfar, M. R. Ali, A. S. Hendy, I. Shah, L. Ali, Localized magnetic fields and their effects on heat transfer enhancement and vortices generation in tri-hybrid nanofluids: A novel investigation, *Case Studies in Thermal Engineering*, pp. 103408, 2023.

[37] S. Ahmad, H. Takana, K. Ali, Y. Akhtar, A. M. Hassan, A. E. Ragab, Role of localized magnetic field in vortex generation in tri-hybrid nanofluid flow: A numerical approach, *Nanotechnology Reviews,* Vol. 12, No. 1, pp. 20220561, 2023.

[38] S. Ahmad, H. Takana, H. G. Castellanos, K. Muzammil, S. Islam, Y. Aryanfar, M. A. Khan, M. Mursaleen, A. S. Hendy, Uncovering the mystery of the vortex dynamics in a micropolar fluid with multiple magnetic field strips: A novel case study, *Case Studies in Thermal Engineering,* Vol. 53, pp. 103716, 2024.

[39] A. Yasmin, K. Ali, M. Ashraf, MHD Casson nanofluid flow in a square enclosure with non-uniform heating using the Brinkman model, *The European Physical Journal Plus,* Vol. 136, No. 2, pp. 1-14, 2021.

[40] T. Shih, C. Tan, B. Hwang, Effects of grid staggering on numerical schemes, *International Journal for numerical methods in fluids,* Vol. 9, No. 2, pp. 193-212, 1989.